AN ELECTRO-OPTIC E-FIELD PROBE

H. Frick, G.V. Meyer
Federal Institute of Technology, Zurich, Switzerland
(Principal contact: gmeyer@nari.ee.ethz.ch)

Abstract: A novel concept for an electric-field (E-field) probe is proposed. The reactive near field, induced by an impinging E-field, of a very short, short-circuited receiving dipole is measured with the aid of an electro-optical modulator. The modulator is designed as a Fabry-Perot etalon. The laser light guided in the etalon is modulated proportionally to the near field of the antenna. The advantage of the etalon is to considerably increase the sensitivity of the probe compared to known electro-optic probes. It is shown analytically, for an ellipsoidal dipole, that only the electrostatic terms of the dipole field are relevant. The advantage of using a dipole much shorter than the wavelength is to minimize the interaction of the probe with the environment and the impinging electromagnetic (EM) field.
Very important is the optimal choice of the material of the modulator. Since the linear electro-optical effect is used, best results are achieved if the index ellipsoid of the material parameters does not rotate under the influence of an external field but only varies its size. Such behaviour is found in materials as e.g. $LiNbO_3$, and poled polymers. Because of reflections, a second parameter of concern is the permittivity of the modulator base material. Its value should be as close as possible to the permittivity of the environment. Therefore, polymers are the most promising materials known today for this kind of probes.

1. Introduction

An EM-field probe acts as a wave-type-transformer from radiated to guided waves. Compared to an antenna it is a non-reciprocal element for the purpose of measuring the characteristics of an impinging EM-field. Among the different physical characteristics of the field only the capture of the one-dimensional electric field with a single probe is theoretically considered. A calibration setup and preliminary measurement results for such an E-field probe are presented in the practical part.
Previous work on field probes using electro-optic transformation has been concentrated on applying modulators at the feeding point of dipoles. To the knowledge of the authors modulators only have been used in the form of Mach-Zehnder interferometer in numerous variations [1]; over 100 patents can be found in the literature. The Mach-Zehnder interferometer should be better replaced by a Fabry-Perot etalon, since the cavity of the etalon considerably increases the sensitivity of the structure. A further amplification of the impinging field is achieved by making use of the field concentration in the close proximity of the antenna structure. In this paper a solution is presented featuring minimal interaction between probe and impinging EM-field, by sacrificing some amount of the dynamic range.

Other remarkable solutions applying electro-optic effects use e.g. a Bragg-structure [2], sectorized electrodes and a Mach-Zehnder interferometer [3], a ring laser using the Faraday effect [4] or a Luneberg-lens to focus the EM-energy [5]. Also a polarizer-analyzer structure with a sphere of electro-optical material has been proposed [6].
The great advantage of the probe described in this paper is its small size, featuring a minimal interaction with the probe and the impinging field, as well as the possibility to realize two and three dimensional sensor arrays. With the aid of such structures the direction of arrival of far fields without ambiguity can be estimated as well as the structure of inhomogeneous EM-fields. By combining such a sensor array and holographic methods a direct visualization of the direction of arrival of a wave front can be realized [7].
In the following we concentrate on the theoretical basics for a small sized E-field probe using an etalon as an electro-optical transformer. Section 2 contains a short description of the principal construction of the near field probe. In section 3 the reactive near field of the probe is analyzed, section 4 is devoted to the material properties for etalons and the characteristics of the probe such as the sensitivity, the bandwidth and the dynamic range. In section 5 a calibration setup and preliminary measurement results for a scaled test sample of such an E-field probe are presented. A more in-depth study of the probe may be found in [8].

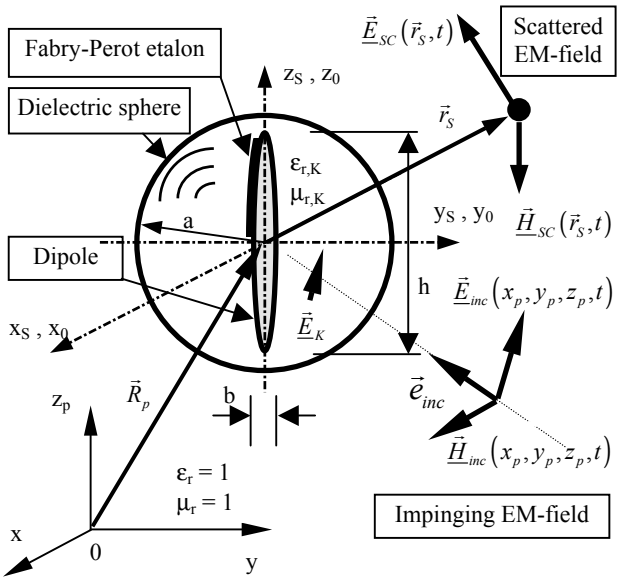

Fig. 1: The E-field probe with dipole and etalon contained in a dielectric sphere.

2. Construction of the probe

The E-field probe consists of an electrical short, short-circuited dipole situated in the centre of a dielectric sphere. The form of the dipole presented in this study is chosen as a rotational ellipsoid (with length h and width b) for the purpose of easy analytical treatment. Any other known form of a dipole may be used but is not considered here. The outline of the probe is shown in Fig. 1. A Fabry-Perot etalon is placed directly on the surface of the dipole. The aim of the dielectric sphere with radius a and relative permittivity $\varepsilon_{r,K}$ is to reduce the gap between the material parameters of etalon and the surroundings ($\varepsilon_r = 1$). The relative permeability μ_r is assumed to be 1 everywhere.

The dielectric sphere is not a prerequisit for the function of the sensor. However by optimising the material parameters of the etalon and the sphere the sensitivity of the probe may be increased.

3. The reactive near field

3.1 Limit of the near field

The electromagnetic field distribution in the vicinity of a short thin dipole shall be considered in this paragraph. The dipole has the form of a prolate ellipsoid and is short circuited (no gap). In the following we concentrate on impinging far fields E_{inc} of the form:

$$\vec{\underline{E}}(x_0,y_0,z_0,t) = \vec{\underline{E}}(x_0,y_0,z_0)\cdot e^{-j\cdot\omega\cdot t} \qquad (1)$$

Let the induction current dnsity J in the dipole be:

$$\vec{\underline{J}}(x_0,y_0,z_0,t) = \vec{\underline{J}}(x_0,y_0,z_0)\cdot e^{-j\cdot\omega\cdot t} \qquad (2)$$

and the corresponding charge density distribution:

$$\underline{\rho}(x_0,y_0,z_0,t) = \underline{\rho}(x_0,y_0,z_0)\cdot e^{-j\cdot\omega\cdot t} \qquad (3)$$

where: $j \equiv \sqrt{-1}$; ω: angular frequency and t: time.

Figure 2 shows the outline of the situation considered.

By introducing the magnetic vector potential $\vec{A}$ and the scalar electric potential φ respectively we can write for the electric field in any point of the space excluding the sources for time harmonic fields of the form (1):

$$\vec{\underline{E}}(x,y,z,t) = j\cdot\omega\cdot\vec{\underline{A}}(x,y,z,t) - grad\left(\underline{\varphi}(x,y,z,t)\right) \qquad (4)$$

Considering a source volume of V the field strength E outside the source region becomes: (5)

$$\vec{\underline{E}}(x,y,z,t) = j\cdot\omega\cdot\frac{\mu_0\cdot\mu_r}{4\cdot\pi}\cdot\iiint_V\frac{\vec{\underline{J}}(x_0,y_0,z_0,t)\cdot e^{j\cdot k\cdot r}}{r}\cdot dx_0dy_0dz_0 -$$

$$\frac{1}{4\pi\varepsilon_0\varepsilon_r}\cdot\begin{bmatrix}\iiint_V\underline{\rho}(x_0,y_0,z_0,t)\cdot[x-x_0]\cdot\left[jk-\frac{1}{r}\right]\cdot\frac{e^{j\cdot k\cdot r}}{r^2}\cdot dx_0dy_0dz_0\\ \iiint_V\underline{\rho}(x_0,y_0,z_0,t)\cdot[y-y_0]\cdot\left[jk-\frac{1}{r}\right]\cdot\frac{e^{j\cdot k\cdot r}}{r^2}\cdot dx_0dy_0dz_0\\ \iiint_V\underline{\rho}(x_0,y_0,z_0,t)\cdot[z-z_0]\cdot\left[j\cdot k-\frac{1}{r}\right]\cdot\frac{e^{j\cdot k\cdot r}}{r^2}\cdot dx_0dy_0dz_0\end{bmatrix}$$

with the wave number: $k = \frac{\omega}{c} = \frac{2\pi}{\lambda}$; the phase velocity: c = $\frac{1}{\sqrt{\varepsilon_0\cdot\varepsilon_r\cdot\mu_0\cdot\mu_r}}$; the electric and the magnetic field constant ε_0 resp. μ_0 and the relative permittivity resp. permeability ε_r and μ_r and wavelength λ. By using the equation of continuity we derive from (5) expressions for the near- and the far field easily identified by the rate of decay with distance r. Since only the field close to the source influences the etalon, we let the field points approaching the source points and compute the field strength at the origin 0. Then the ratio V of the far-field to the near-field term tends to:

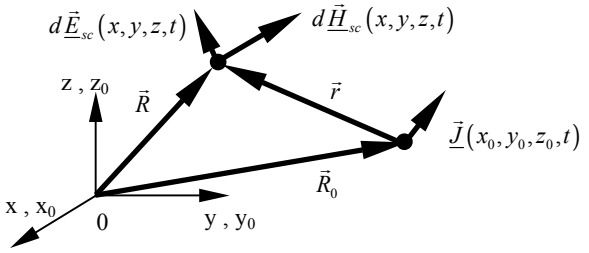

Fig. 2: Coordinate system.

$$\underline{V} = \frac{\underline{E}_{far}}{\underline{E}_{near}} = \frac{[k\cdot r]^2}{j\cdot k\cdot r - 1} \qquad (6)$$

A sphere with the radius: $r = \frac{\lambda}{2\pi}$ is defining the surface where the far- and the near-field terms are of equal strength. By only looking at the near field term and using:

$$\vec{r} = \vec{R} - \vec{R}_0 = \begin{bmatrix}x-x_0\\ y-y_0\\ z-z_0\end{bmatrix} \Rightarrow$$

$$|\vec{r}| = r = \sqrt{[x-x_0]^2+[y-y_0]^2+[z-z_0]^2}$$

the complex near field deduced from (5) yields:

$$d\vec{\underline{E}}(x,y,z,t)_{near} = -\frac{1}{4\pi\varepsilon_0\varepsilon_r}\cdot\underline{\rho}(x_0,y_0,z_0,t)\cdot[jkr-1]\cdot$$

$$\frac{\cos(kr)+j\cdot\sin(kr)}{r^3}\cdot dx_0dy_0dz_0\cdot\vec{r} \qquad (7)$$

With

$$\mathrm{Re}\left\{d\vec{\underline{E}}(x,y,z)_{near}\right\} = \frac{\rho(x_0,y_0,z_0)\cdot dx_0dy_0dz_0}{4\cdot\pi\cdot\varepsilon_0\cdot\varepsilon_r}\cdot\frac{\vec{r}}{r^3}\cdot F_{\mathrm{Re}}$$

$$\mathrm{Im}\left\{d\vec{\underline{E}}(x,y,z)_{near}\right\} = -\frac{\rho(x_0,y_0,z_0)\cdot dx_0dy_0dz_0}{4\cdot\pi\cdot\varepsilon_0\cdot\varepsilon_r}\cdot\frac{\vec{r}}{r^3}\cdot F_{\mathrm{Im}}$$

where

$$F_{\mathrm{Re}} = k\cdot r\cdot\cos(k\cdot r)+\sin(k\cdot r)$$

$$F_{\mathrm{Im}} = k\cdot r\cdot\cos(k\cdot r)-\sin(k\cdot r)$$

the ratio N of the imaginary term to the real term becomes:

$$N = \frac{F_{\mathrm{Im}}}{F_{\mathrm{Re}}} = \frac{k\cdot r\cdot\cos(k\cdot r)-\sin(k\cdot r)}{k\cdot r\cdot\sin(k\cdot r)+\cos(k\cdot r)} \qquad (8)$$

If |N| << 1 , the real part of the near field is dominant. In the next step it is required that the frequency-dependent part of F_{Re} should be negligibly small, M<<1:

$$M = \frac{M_{kr}}{M_{stat}} = \frac{k\cdot r\cdot\sin(k\cdot r)}{\cos(k\cdot r)} = k\cdot r\cdot\tan(k\cdot r) \qquad (9)$$

If the following four inequalities are valid:

1) $|\underline{V}| << 1$: the far field term can be neglected

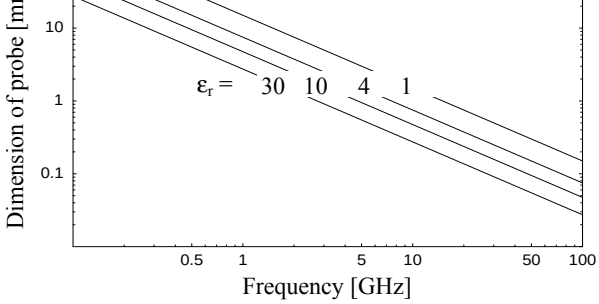

Fig. 3: Maximum dimension of the probe for the assumption of static field conditions.

2) $|N| << 1$: the imaginary part of the near field can be neglected

3) $M << 1$: the term M_{kr} in (9) can be neglected

4) $W = 1 - \cos(k \cdot r) \approx 0$ makes M proportional $(k\,r)^2$

the electromagnetic field in the near proximity of a small source may be described with sufficient small errors by the formulas for static fields:

Electric charge: $dQ(x_0, y_0, z_0) = \rho(x_0, y_0, z_0) \cdot dx_0 dy_0 dz_0$

Quasi-static field: $d\underline{\vec{E}}(x, y, z, t) \approx d\underline{\vec{E}}(x, y, z) \cdot e^{-j \cdot \omega \cdot t}$

Electrostatic field $d\underline{\vec{E}}(x, y, z) = \frac{dQ(x_0, y_0, z_0)}{4 \cdot \pi \cdot \varepsilon_0 \cdot \varepsilon_r} \cdot \frac{\vec{r}}{r^3}$ (10)

The most stringent condition applies for M. As long as the product kr is less than 0.3, the difference between the assumed electrostatic field and the real field is less than 10%. It can be shown [9] that for the magnetic field the same limits exist for the assumption of the magneto-static field.

By assuming a relative permeability μ_r=1 of the surrounding material of the dipole and varying the relative permittivity ε_r we receive an estimated maximum dimension of the probe leading to a systematic deviation of 10% between static and dynamic field strength (see Fig. 3).

3.2 Field distribution in the vicinity of the dipole

Having analysed the extension of the near field we can determine the length of the dipole such that it is completely contained in the quasi-static near field. As shown it is then sufficient to use only the static field term. Furthermore we can assume to have a homogeneous plane wave impinging on the dipole.

3.2.1 Parallel field

First we consider the situation of a TEM wave with the E-field vector parallel to the main axis of the dipole. For ease of computation we choose a prolate spheroidal coordinate system (η, θ, ψ) as shown in Fig. 4.

Assuming an impinging field of the form:

$$\vec{E}_0 = \begin{bmatrix} E_x \\ E_y \\ E_z \end{bmatrix} = \begin{bmatrix} 0 \\ 0 \\ -E_0 \end{bmatrix} \quad (11)$$

We get for the scalar electric potential ϕ_1 [9]:

$$\phi_1(\eta, \theta, \psi) = \sum_{n=0}^{\infty} \left[B_n P_n \cosh(\eta) + C_n Q_n \cosh(\eta) \right] \cdot P_n \cos(\theta) \quad (12)$$

$$x = a \cdot \sinh(\eta) \cdot \sin(\theta) \cdot \cos(\psi)$$
$$y = a \cdot \sinh(\eta) \cdot \sin(\theta) \cdot \sin(\psi)$$
$$z = a \cdot \cosh(\eta) \cdot \cos(\theta)$$

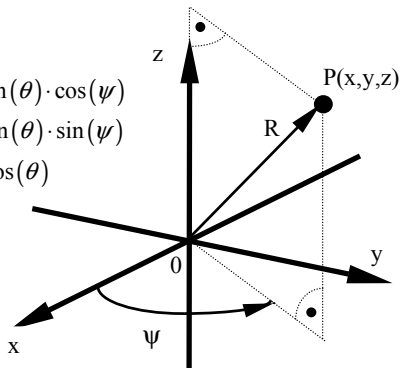

Fig. 4: Prolate spheroidal coordinate system.

where P_i indicate Legendre polynoms of the first kind, Q_i of the second kind, respectively. The boundary conditions have to be satisfied and since the electrostatic field is proportional to the gradient of the scalar potential we get from (12) an expression for the electric field in the proximity of the dipole in case of parallel polarisation:

$$E_\eta(\eta, \theta, \psi) = -\frac{E_0 \cdot \cos(\theta)}{\sqrt{\left[\sinh(\eta)\right]^2 + \left[\sin(\theta)\right]^2}} \cdot \left[\sinh(\eta) - \frac{\cosh(\eta_0)}{Q_1(\cosh(\eta_0))} \cdot Q_1'(\cosh(\eta)) \right]$$

$$E_\theta(\eta, \theta, \psi) = \frac{E_0 \cdot \sin(\theta)}{\sqrt{\left[\sinh(\eta)\right]^2 + \left[\sin(\theta)\right]^2}} \cdot \left[\cosh(\eta) - \frac{\cosh(\eta_0)}{Q_1(\cosh(\eta_0))} \cdot Q_1(\cosh(\eta)) \right] \quad (13)$$

$$E_\psi(\eta, \theta, \psi) = 0$$

On the surface of the dipole we deduce from (13) that only the component E_η exists.

The increase of the field component E_η relative to the free field E_0 for the ratio of the short to the long axis of the dipole b/h = 0.01 is between 100 to 1000 over about 2/3 of the extension of the dipole [8].

The equipotential lines surrounding the dipole may be seen in Fig. 5. An estimate of the size of the surrounding dielectric sphere may also be gained from this figure since the assumption of static field requires having parallel equipotential lines at the inner surface of the sphere.

3.2.2 Perpendicular fields

For an impinging electric far field perpendicular polarized to the main axis of the ellipsoidal dipole, the latter may be replaced by an infinitesimal cylinder. This is a reasonable assumption in case of a thin ellipsoid in the centre region of the dipole, but the effects of the ends are not considered.

At the surface of the cylinder the only remaining field component is:

$$E_r(r = b, \beta, z) = E_0 \cdot 2 \cdot \cos(\beta) \quad (14)$$

This means we only have a radial field component featuring a cosine function along the perimeter of the cylinder with a maximum value of two times the far field strength.

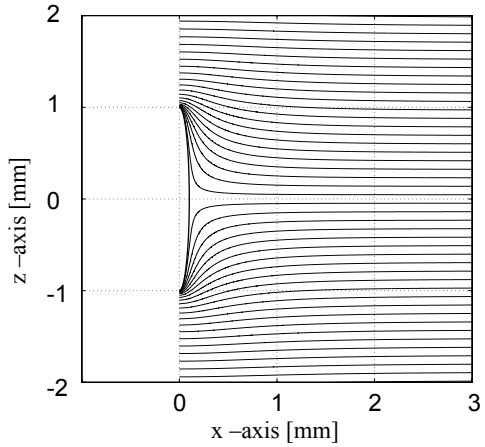

Fig. 5: Equipotential lines around the dipole with b/h=0.1.

4. The electrooptic transducer

Instead of capturing the induced voltage at the gap of an antenna, the new idea realized with this probe is to make use of the enhanced quasistatic field in the proximity of the dipole

periphery. This field directly acts on an electrooptical modulator consisting of an optical waveguide of length L_E. Optical modulators make use of the linear electrooptic effect. A considerable increase of the sensitivity of the modulator can be achieved by replacing the modulator with a Fabry-Perot etalon consisting of a modulator featuring two semipermeable mirrors at the ends.

4.1 The Fabry-Perot etalon

The principle of the Fabry-Perot etalon is shown in Fig. 6. A light wave E_{IN} guided by an optical fibre is impinging on the etalon from the left side. The etalon consists of two semipermeable mirrors and a piece of electro-optic material of the length L_E (modulator). An external EM field modulates the refractive index of the electro-optic material and therefore the propagation velocity of the light wave E_{IN}. The superposition of the multiple reflections and transmissions on mirror 1 leads to the resulting reflected light wave E_{OUT} in the optical fibre.

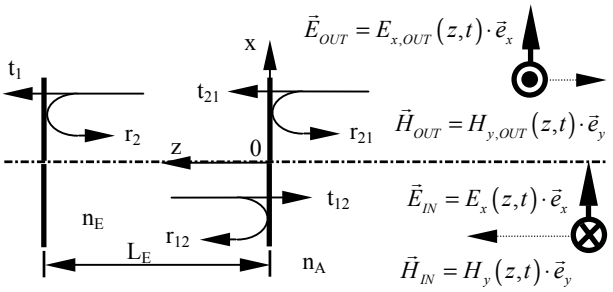

Mirror 2 Modulator Mirror 1 Optical fibre

Fig. 6: Principle of the Fabry-Perot etalon.

The meaning of the symbols in Fig. 6 is the following:

t_1 , t_{12} , t_{21}	: value of the amplitude transmission coefficients at the mirror 1, $\in \Re$
r_2 , r_{12} , r_{21}	: value of the amplitude reflection coefficients at the mirrors, $\in \Re$
n_E	: refractive index of the modulator base material, $\in \Re$
n_A	: refractive index of the optical fibre, $\in \Re$
L_E	: length of the etalon

The etalon may be approximated by a linear dispersionless system and therefore Fourier techniques are applicable. Given the impulse response $h_{Etalon\text{-}R}(t)$ respective the transfer function $H_{Etalon\text{-}R}(\omega)$ at the mirror 1 or at z = 0 , in Fig. 6., the field strength resulting from the superposition of plane waves is given as:

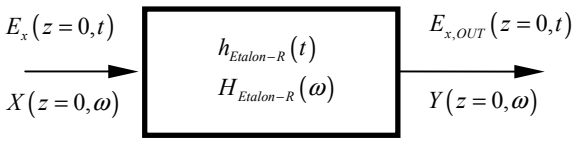

$$E_{x,OUT}(z=0,t) = r_{21}\cdot E_x(z=0,t) \quad + \quad [t_{12}\cdot t_{21}\cdot r_2]\cdot\sum_{m=0}^{\infty}[r_{12}\cdot r_2]^m\cdot E_x(z=0,t-2\cdot[m+1]\cdot\tau_E) \tag{15}$$

featuring a Fouriertransform Y of:

$$Y(z=0,\omega) = r_{21}\cdot X(z=0,\omega) \quad + \quad [t_{12}\cdot t_{21}\cdot r_2]\cdot \sum_{m=0}^{\infty}[r_{12}\cdot r_2]^m\cdot X(z=0,\omega)\cdot e^{-j\cdot\omega\cdot 2\cdot[m+1]\cdot\tau_E}$$

$$\Rightarrow\ Y(z=0,\omega) = \left[r_{21} \quad + \quad t_{12}t_{21}r_2e^{-j\cdot\omega\cdot 2\cdot\tau_E}\cdot\frac{1}{1-r_{12}r_2e^{-j\cdot\omega\cdot 2\cdot\tau_E}}\right]\cdot X(z=0,\omega) \tag{16}$$

where the transition time τ_E is given by:

$$\tau_E = \frac{L_E}{c_0}\cdot n_E$$

The frequency response of the etalon now may be computed from: (17)

$$H_{Etalon-R}(\omega) = \frac{Y(z=0,\omega)}{X(z=0,\omega)} = r_{21} + t_{12}t_{21}r_2\cdot\frac{e^{-j\cdot\omega\cdot 2\cdot\tau_E}}{1-r_{12}r_2e^{-j\cdot\omega\cdot 2\cdot\tau_E}}$$

resp. for the intensities of the light wave:

$$\left|H_{Etalon-R}(\omega)\right|^2 = [r_{21}]^2 + \frac{2\cdot r_{21}\cdot t_{12}\cdot t_{21}\cdot r_2\cdot[\cos(\omega\cdot 2\cdot\tau_E) - r_{12}\cdot r_2] + [t_{12}\cdot t_{21}\cdot r_2]^2}{1-[r_{12}\cdot r_2]\cdot 2\cdot\cos(\omega\cdot 2\cdot\tau_E) + [r_{12}\cdot r_2]^2}$$

Assuming a monochromatic TEM light wave E_{IN} (see Fig. 6) the reflection coefficient R is also given by the intensity of the reflected wave I_R relative to the intensity of the impinging light I_{IN}:

$$R = \frac{I_R}{I_{IN}} = [r_{21}]^2 + \frac{2r_{21}[t_{12}]^2 r_2\left[\cos\left(4\pi\frac{L_E}{\lambda_0}n_E\right) + r_{21}r_2\right] + [t_{21}]^4[r_2]^2}{1+[r_{21}r_2]2\cos\left(4\pi\frac{L_E}{\lambda_0}n_E\right) + [r_{21}r_2]^2} \tag{18}$$

with the free space light wavelength λ_0 and the condition of the conservation of the energy:

$$t_{21} = t_{12} \quad ; \quad r_{21} = -r_{12} \quad ; \quad [t_{21}]^2 + [r_{21}]^2 = 1\,.$$

Interesting for the application of modulators is the sensitivity of R to small changes of the refractive index Δn: $R(n_{E0} + \Delta n)$

The computed sensitivity of the etalon is shown in Fig. 7 assuming $r_2 = -r_{21}$ and introducing the variable Λ:

$$\Lambda = 4\cdot\pi\cdot\frac{L_E}{\lambda_0}\cdot n_{E0} \tag{19}$$

The etalon has a 2π periodic reflection behaviour in the form of a filter. With increasing reflection r_2 at the end of the etalon the transmission region gets smaller and steeper. In addition the sensitivity of the etalon to small changes of the refractive index increases considerably. With increasing length of the etalon L_E, also the sensitivity increases.

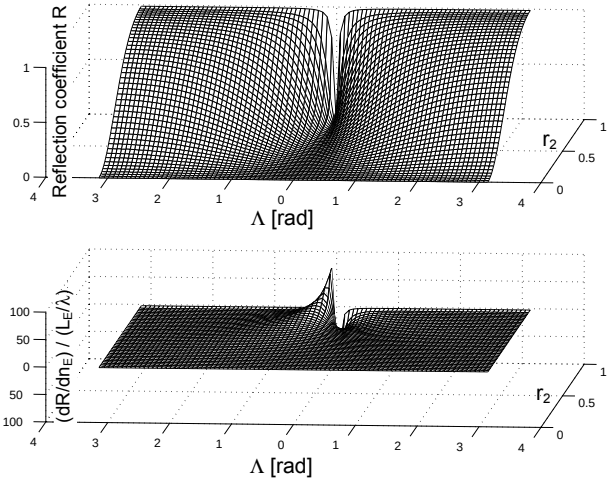

Fig. 7: Characteristics of the reflection coefficient and the sensitivity as a function of the reflection at the end of the etalon and some characteristic measures of the etalon Λ.

4.2 The linear electrooptical effect

If a material shows a linear dependency between an applied electric field and the optical refractive index it is called a linear electrooptic material. The linear electrooptic effect only

exists in crystals that do not possess inversion symmetry. The propagation characteristics in crystals are fully described by means of the index ellipsoid which may be expressed as [10]:

$$\frac{[x_1]^2}{[n_1]^2} + \frac{[x_2]^2}{[n_2]^2} + \frac{[x_3]^2}{[n_3]^2} = 1 \qquad (20)$$

Given an external electric field E:

$$\vec{E} = \begin{bmatrix} E_x \\ E_y \\ E_z \end{bmatrix} = \begin{bmatrix} E_1 \\ E_2 \\ E_3 \end{bmatrix}$$

the index ellipsoid changes according to:

$$1 = \eta_{11}(E_1,E_2,E_3)[x_1]^2 + \eta_{22}(E_1,E_2,E_3)[x_2]^2 + \eta_{33}(E_1,E_2,E_3)[x_3]^2 + \\ + \eta_{12}(E_1,E_2,E_3)x_1x_2 + \eta_{21}(E_1,E_2,E_3)x_2x_1 + \eta_{13}(E_1,E_2,E_3)x_1x_3 + \\ + \eta_{31}(E_1,E_2,E_3)x_3x_1 + \eta_{23}(E_1,E_2,E_3)x_2x_3 + \eta_{32}(E_1,E_2,E_3)x_3x_2 \qquad (21)$$

As can be expected in a general case from eq. 21, the index ellipsoid is changed and rotated under the influence of an external field. This results in cross terms and a split of the impinging field in ordinary and extraordinary rays, what is called birefringence. Anisotropic materials suitable for modulation purposes in information carrying systems must be approximated by an index ellipsoid according to:

$$1 = \eta_1(E_1,E_2,E_3)[x_1]^2 + \eta_2(E_1,E_2,E_3)[x_2]^2 + \eta_3(E_1,E_2,E_3)[x_3]^2 \qquad (22)$$

Provided the following inequations are valid:

$$[r_{11}\cdot E_1 + r_{12}\cdot E_2 + r_{13}\cdot E_3]\cdot[n_1]^2 \ll 1 \quad ; \\ [r_{21}\cdot E_1 + r_{22}\cdot E_2 + r_{23}\cdot E_3]\cdot[n_2]^2 \ll 1 \quad ; \qquad (23) \\ [r_{31}\cdot E_1 + r_{32}\cdot E_2 + r_{33}\cdot E_3]\cdot[n_3]^2 \ll 1$$

the change of the refractive indices under the influence of an external electromagnetic field of such materials may be approximated with:

$$n_1(E_1,E_2,E_3) \approx n_1 + \Delta n_1 \quad ; \\ with \quad \Delta n_1 = -\frac{1}{2}\cdot[r_{11}\cdot E_1 + r_{12}\cdot E_2 + r_{13}\cdot E_3]\cdot[n_1]^3 \\ n_2(E_1,E_2,E_3) \approx n_2 + \Delta n_2 \quad ; \\ with \quad \Delta n_2 = -\frac{1}{2}\cdot[r_{21}\cdot E_1 + r_{22}\cdot E_2 + r_{23}\cdot E_3]\cdot[n_2]^3 \qquad (24) \\ n_3(E_1,E_2,E_3) \approx n_3 + \Delta n_3 \quad ; \\ with \quad \Delta n_3 = -\frac{1}{2}\cdot[r_{31}\cdot E_1 + r_{32}\cdot E_2 + r_{33}\cdot E_3]\cdot[n_3]^3$$

In the literature two materials can be found suitable for Fabry-Perot etalons: $LiNbO_3$ and poled polymers. Widely used today is $LiNbO_3$ featuring an electrooptic tensor of:

$$r_{LiNbO_3}(\lambda_0 = 633nm) = \begin{bmatrix} 0 & -3.4 & 8.6 \\ 0 & 3.4 & 8.6 \\ 0 & 0 & 30.8 \\ 0 & 28 & 0 \\ 28 & 0 & 0 \\ -3.4 & 0 & 0 \end{bmatrix} \left[\frac{pm}{V}\right] \qquad (25)$$

at an optical wavelength of 633 nm. The drawbacks of $LiNbO_3$ are a moderate figure of merit and a high permittivity of about ε_r=30.

4.3 The sensitivity of the probe

For the investigation of the sensitivity an optical waveguide of the length L_E consisting of electrooptic material and guiding linear polarized monochromatic light is considered. The change of the intensity reflection coefficient R under the influence of an external electromagnetic field is of primary interest if this waveguide is used as a modulator. The light wave shall be described by:

$$\vec{E}_{opt} = \begin{bmatrix} E_{1,opt} = 0 \\ E_{2,opt} = 0 \\ E_{3,opt} \end{bmatrix} \qquad (26)$$

and the electromagnetic field by:

$$\vec{E}(x_1) = \begin{bmatrix} E_1(x_1) \\ E_2(x_1) \\ E_3(x_1) \end{bmatrix} \qquad (27)$$

correspondingly. Given a material fulfilling eq. 24 and in addition:

$$[n_3]^2 r_{31}E_1(x_1) + [n_3]^2 r_{32}E_2(x_1) + [n_3]^2 r_{33}E_3(x_1) \ll 1$$

the tensor of the refractive index is reduced to n_3:

$$n_3(E_{1,eff},E_{2,eff},E_{3,eff}) = n_3 + \Delta n_{3,eff}(E_{1,eff},E_{2,eff},E_{3,eff})$$

with

$$\Delta n_{3,eff}(E_{1,eff},E_{2,eff},E_{3,eff}) = -\frac{1}{2}[n_3]^3\left[r_{31}E_{1,eff} + r_{32}E_{2,eff} + r_{33}E_{3,eff}\right]$$

and

$$\Rightarrow E_{1,eff} = \frac{1}{L_E}\cdot\int_0^{L_E} E_1(x_1)\cdot dx_1 \\ \Rightarrow E_{2,eff} = \frac{1}{L_E}\cdot\int_0^{L_E} E_2(x_1)\cdot dx_1 \qquad (28) \\ \Rightarrow E_{3,eff} = \frac{1}{L_E}\cdot\int_0^{L_E} E_3(x_1)\cdot dx_1$$

For the operation of the Fabry-Perot etalon the amount of change of the light reflection is of primary interest. From eq. 18 we may deduce:

$$R\left(n_3 + \Delta n_{3,eff}(E_{1,eff},E_{2,eff},E_{3,eff})\right) \approx R(r_{21},r_2,t_{12},L_E,\lambda_0,n_3) + \\ \frac{d}{dn_E}R(r_{21},r_2,t_{12},L_E,\lambda_0,n_E)\Big|_{n_E=n_3}\cdot\Delta n_{3,eff}(E_{1,eff},E_{2,eff},E_{3,eff}) \qquad (29)$$

Now setting $E_{1,eff}$ = 0, $E_{2,eff}$ = 0 and n_{E0}=n_3, an expression for the contrast K_K of the etalon is achieved where the contrast is defined by the second term of eq. 29:

$$I_R = R\cdot[1 + K_K]\cdot I_{Ein} \qquad (30)$$

$$\text{with the contrast:} \quad K_K = \frac{W_S\cdot\frac{\left[[n_3]^3\cdot r_{33}\right]}{\lambda_0}\cdot\int_0^{L_E} E_3(x_1)\cdot dx_1}{R}$$

$$R = R(r_{21},r_2,t_{12},\Lambda) = \\ [r_{21}]^2 + \frac{2\cdot r_{21}\cdot[t_{12}]^2\cdot r_2\cdot[\cos(\Lambda) + r_{21}\cdot r_2] + [t_{21}]^4\cdot[r_2]^2}{1 + [r_{21}\cdot r_2]\cdot 2\cdot\cos(\Lambda) + [r_{21}\cdot r_2]^2} \qquad (31)$$

$$W_S = -\frac{[r_{21}\cdot r_2]\cdot\sin(\Lambda)\cdot 4\cdot\pi}{1 + [r_{21}\cdot r_2]\cdot 2\cdot\cos(\Lambda) + [r_{21}\cdot r_2]^2}\cdot \\ \left[\frac{2\cdot r_{21}\cdot[t_{12}]^2\cdot r_2\cdot[\cos(\Lambda) + r_{21}\cdot r_2] + [t_{21}]^4\cdot[r_2]^2}{\left[1 + [r_{21}\cdot r_2]\cdot 2\cdot\cos(\Lambda) + [r_{21}\cdot r_2]^2\right]} - [t_{12}]^2\right] \qquad (32)$$

Λ is defined by eq. 19. Assuming an impinging field E_K inside the dielectric sphere or E_0 outside (see Fig. 1) parallel to the main axis of the probe:

$$\vec{E}_K = -E_K\cdot\vec{e}_z = \frac{3}{\varepsilon_{r,K} + 2}\cdot E_0\cdot\vec{e}_z \qquad (33)$$

and again using prolate spheroidal coordinates, the contrast K_S for a thin ellipsoidal dipole (b/h ≤ 0.05) may be approximated by:

$$I_R = R \cdot [1 \quad + \quad K_S] \cdot I_{Ein}$$

$$K_S(E_K) = \frac{W_S \cdot M_S \cdot N_S}{R} \cdot E_K$$

$$N_S = -\left[\sinh(\eta_0) - \frac{\cosh(\eta_0)}{Q_1(\cosh(\eta_0))} \cdot Q_1'(\cosh(\eta_0)) \right] \quad (34)$$

$$\eta_0 = \operatorname{arctanh}\left(\frac{b}{h}\right)$$

$$M_S = \left[[n_3]^3 \cdot r_{33} \right] \cdot \frac{c}{\lambda_0}$$

The sensitivity of a probe using for example $LiNbO_3$ for the electrooptic material of the etalon now can be estimated. By selecting an ellipsoidal dipole with b/h = 0.01, a reflectivity of the etalon of $r_2 = 0.995$ and the normalized contrast $K_{Sn} = 10^5$: The figure of merit for $LiNbO_3$ is about 330 10^{-12} V/m and the permittivity $\varepsilon_{r,K}$= 30. If we choose the optical wavelength λ_0 = 633 nm for the laser source, then we get from eq. 37:

$$K_S = \left[10^5 \cdot 330 \cdot 10^{-12} \cdot 2765 \right] \cdot E_K \quad \approx \quad 0.09 \cdot E_K$$

If we assume in addition that the photodetector is able to detect a minimal contrast K = 0.01, then from eq. 36 we receive the result that a minimum field strength for the parameters assumed of:

$$E_{K,MIN} \cdot \frac{\varepsilon_{r,K} + 2}{3} = E_{0,MIN} = \frac{0.01}{0.09} \cdot \frac{30 + 2}{3}$$

$$\Rightarrow \quad \underline{\underline{E_{0,MIN} \approx 1 \quad \frac{V}{m}}}$$

can be detected. This value certainly can be lowered considerably by optimizing the etalon.

5. Probe measurements

Since etalons of a suitable dimension are not available on the market, for first experiments the etalon has been replaced by an unpacked and pigtailed electrooptic modulator combined with a directional optical coupler (see Fig. 8). For optimal signal stacking all optical parts in the loop have to be polarization maintaining.

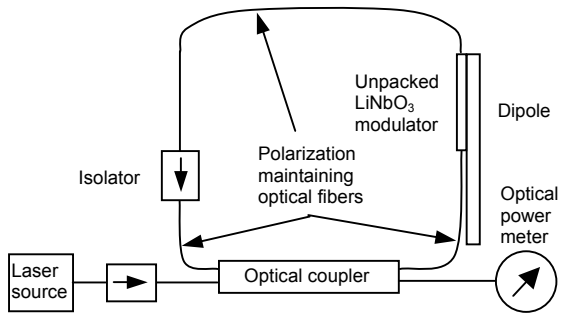

Fig. 8: Preliminary setup of the electro-optic E-field probe.

Currently tests with the probe as seen in Fig. 8 are performed in the TEM field of an eccentric triplate line as shown in Fig. 9.

6. Conclusions and outlook

In this preliminary study about a new electromagnetic field probe using a short dipole and a Fabry-Perot etalon as electro-optic transducer, it has been theoretically proved that very large bandwidths and high sensitivity may be realized. The bandwidth theoretically starts at DC and stops at several GHz depending on the technology applied all with one probe. Easily realizable is a sensitivity of 1 V/m, for higher sensitivities an optimization of the probe has to be performed, especially for the material of the etalon.

By using more than one etalon per probe and some signal manipulation at the receiver the cross polarized field components may be suppressed. Furthermore by applying probes in different orientations the vector-field may be picked up.

This work is based on the ND thesis [9].

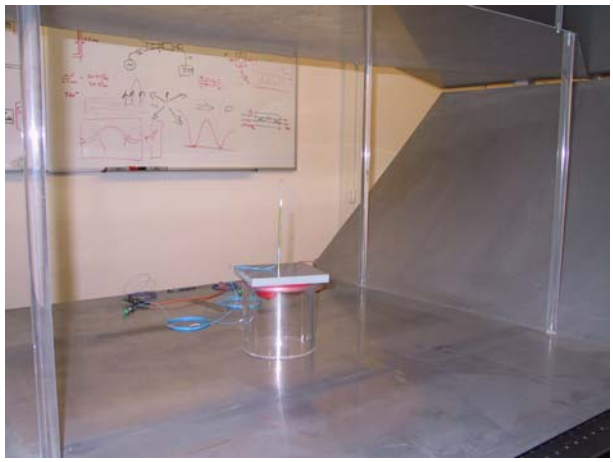

Fig. 9: Test and calibration setup for the E-field probe.

References

[1] C. Saam: Feld Sensor - Patent Publications**,** SCHAF-R-5; P&TS, Patents & Technology Surveys, Neuchatel, Feb. 20, 2002.

[2] Electric field sensor for controllers of computer, communication apparatus, Japanese patent No JP11194146, March 24, 1998.

[3] K. Hayeiwa, T. Ishikawa, M. Kondo, H. Naka, Y. Sato, Y. Toba: Electric field sensor for electromagnetic wave, e.g. radio receptrion, Japanese patent No JP07306235, May 12, 1994.

[4] Electromagnetic field measuring device has ring laser which is used as electromagnetic field sensor; Japanese patent No JP2001281272, March 3, 2000.

[5] D. P. Hilliard, D. L. Mensa: Photonic EM field sensor for incident planar EM wave; US patent No US5225668, July 6, 1991.

[6] P. A. Schollet: Electric field sensor using Pockels effect on crystal sphere; European patent No EP0453693, Dec. 21, 1990.

[7] H. Frick: Entwurf einer Zonenlinsenantenne für breitbandige Funkkanalmessungen; Diploma theses No 333, CTL ETH Zurich, 1999.

[8] G. Meyer, H. Frick: A novel E-field probe; submitted to the IEEE Trans. on AP, 2002.

[9] H. Frick: Entwicklung eines Feldsensors; ND theses, CTL ETH Zurich, 2002.

[10] B. E. A. Saleh, M. C. Teich: Fundamentals of Photonics*;* John Wiley & Sons, INC. , 1991.